Effects of Pyrolysis Temperature of Macroalgal Biomass on the Structure and Mechanical Properties of Produced Biochar

Brandon Lou [†], Mallory Parker [†], and Eleftheria Roumeli *

[†]*Contributed equally to this manuscript and share the first author role*
**Corresponding author: eroumeli@uw.edu*

DOI: 10.15376/biores.20.2.4152-4173

GRAPHICAL ABSTRACT

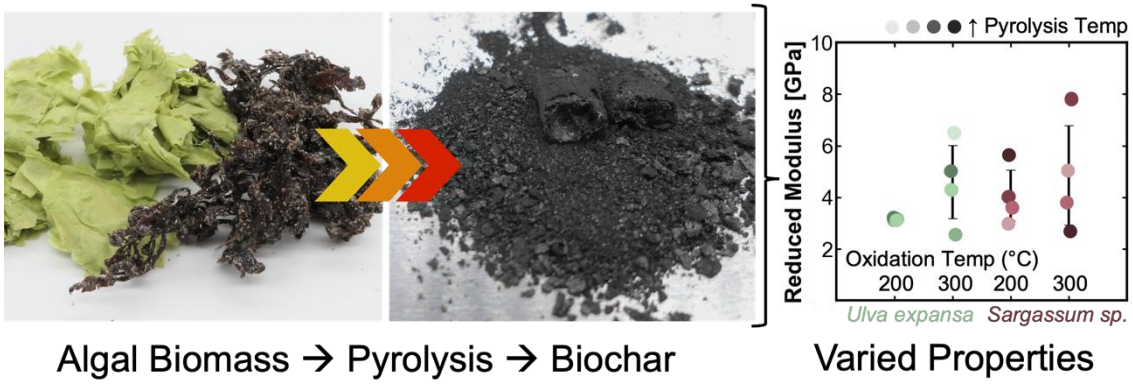

Effects of Pyrolysis Temperature of Macroalgal Biomass on the Structure and Mechanical Properties of Produced Biochar

Brandon Lou ,† Mallory Parker ,† and Eleftheria Roumeli *

Biochars, produced *via* pyrolysis, are gaining attention in applications ranging from soil amendments to energy storage and environmental remediation. While lignocellulosic biochars from woody biomass are well studied, algal biochars remain comparatively overlooked despite offering diverse organic and inorganic content that may broaden their applications. This study investigates how pyrolysis temperature and oxidative pretreatment affect the structure and properties of biochars derived from two macroalgae, *Ulva expansa* and *Sargassum* sp., under various pyrolysis conditions (500 to 900 °C). Using Raman spectroscopy, X-ray photoelectron spectroscopy, X-ray diffraction, scanning electron microscopy, and nanoindentation, it was found that the C-O and C-N surface functional groups decreased in *Ulva* but the C=O and C-O-C groups increased in *Sargassum* upon pyrolysis. The reduced modulus ranged between 2.6 to 7.9 GPa and was governed by pyrolytic carbon content and inorganic composition. Of these two factors, the amount and type of pyrolytic carbon were determined by the heating conditions, with oxidation at 200 °C generally preserving more carbon than oxidation at 300 °C. Meanwhile, the final pyrolysis temperature dictated residual carbon content, salt formation, and carbonation. These findings highlight the potential for tailored pyrolysis to produce algal biochars with customizable structures and properties, enabling environmental and industrial applications such as carbon sequestration, filtration, and energy storage.

DOI: 10.15376/biores.20.2.4152-4173

Keywords: Biochar; Biomass pyrolysis; Macroalgae; Oxidation

*Contact information: Department of Materials Science and Engineering, University of Washington, Box 352120, Seattle, WA, USA 98195-21120; †Contributed equally to this manuscript and share the first author role; *Corresponding author: eroumeli@uw.edu*

INTRODUCTION

Climate change is a global challenge that drives the pursuit of sustainable solutions to reduce greenhouse gas emissions and dependence on fossil fuels (Dietz *et al.* 2020). Such solutions include circular economy practices, expanded recycling capabilities, carbon capture technologies, and the use of renewable energy (Malhi *et al.* 2020; Lin *et al.* 2021). Biomass has gained attention as a resource for fuels, chemicals, and bioproducts – including biochar – because of its abundance, chemical diversity of feedstock materials, resultant range of bioproducts, the possibility of achieving carbon-neutrality, and overall its sustainability premise.

Not only can biofuels be an alternative to petrochemicals (Rodionova *et al.* 2017), but other bioproducts such as biochars can be used in a variety of applications such as wastewater treatment (Bhatnagar *et al.* 2021), catalysis (Cao *et al.* 2021), and even electronic applications (Roche *et al.* 2023). Another sustainability opportunity for biochar lies in the feedstock selection. When considering biomass sources to derive biochar, algal species can and have been used (Song *et al.* 2019; Jayathilake *et al.* 2024). Furthermore, considering that contaminated or invasive algal species pose threats to the marine ecosystem, their removal and utilization to create bioproducts offers added potential benefits for the sourcing ecosystem. Recent governmental and research initiatives highlight the growing interest in macroalgae as a renewable feedstock. For instance, a recent report the U.S. Department of Energy identifies seaweeds as a promising resource for CO_2 removal and bioproduct synthesis, while the Environmental Protection Agency recognizes *Sargassum* inundation events as disruptive to coastal ecosystems and seeks mitigation strategies (Coleman *et al.* 2024; US EPA 2023). In many coastal areas, large blooms of invasive seaweeds are already collected by local authorities, providing a readily available biomass that can be converted to biochar and other value-added products. Meanwhile, research efforts into cultivating macroalgae in controlled, impounded water systems (*e.g.*, "hydroponic" approaches) are also expanding to address demand for large-scale sustainable feedstocks (Revilla-Lovano *et al.* 2021).

Pyrolysis is the most common approach to prepare biochar from biomass (Cao *et al.* 2021; El-Gendy *et al.* 2024). In a pyrolysis process the thermal decomposition of a material occurs in an oxygen free (inert, usually nitrogen or vacuum) atmosphere. Biomass pyrolysis generally occurs in three distinct stages: removal of moisture, thermal degradation of organic components (polymers like carbohydrates, lower molecular weight sugars, lipids, and proteins), which can occur in one or more distinct temperature ranges depending on the molecular weight, polymer composition and structure, and lastly the region with constant residual mass corresponding to the inorganic components that do not thermally decompose in the studied ranges (salts, or inorganic elements in organic compounds) (Peng *et al.* 2000). The final product of biomass pyrolysis is a solid residue referred to as biochar, as well as bio-oil in liquid phase and syngas in gaseous phase (Jahirul *et al.* 2012; Mong *et al.* 2022). Altering the heating rate, temperature profile, and other parameters effectively changes the pyrolysis stages to ultimately control the amount and structure of carbon in the solid residue, as well as the overall organics content. Specifically, the variation of heating rate classifies a pyrolysis technique as slow, fast, or flash (Fahmy *et al.* 2018), and the heating rate used will impact the final products achieved. Slow pyrolysis has been shown in woody biomass to yield the largest amount of biochar compared to fast or flash pyrolysis (Jesus *et al.* 2020), and is therefore implemented in this study. Biochars from pyrolysis are of interest for their rich carbon content and physicochemical properties, which can be valuable for applications in energy storage and soil amendments (Singh *et al.* 2010; Roche *et al.* 2023), in addition to previously mentioned environmental remediation (Bhatnagar *et al.* 2021).

Many feedstocks, ranging from agricultural residues to wood and macroalgae, have been studied as biochar sources (Ross *et al.* 2008, Das *et al.* 2015). Table 1 summarizes relevant literature on biochar yields from a variety of materials (including rice straw, wood bark, and various macroalgae) and details their heating rates, final pyrolysis temperatures, and residence times.

Table 1. Comparison of Biochars Produced through Pyrolysis of Different Source Materials

Biomass Type	Pyrolysis Temp. (°C)	Heating Rate (°C/min)	Residence Time (min)	Yield (%)	Notes	Source
Rice straw	300 to 700	10	120	31.1 to 48.8		Tu *et al.* 2022
Corn straw	300 to 700	10	120	22.7 to 35.4		Tu *et al.* 2022
Camellia oleifera shells	300 to 700	10	120	32.4 to 50.7		Tu *et al.* 2022
Garden waste	300 to 700	10	120	25.1 to 42.6		Tu *et al.* 2022
Rice husk	180	n/a	20	57.9	Hydrothermal, 70 bar	Hossain *et al.* 2020
Bagasse	500	10	> 60	24.5		Lee *et al.* 2013
Cocopeat	500	10	> 60	38.7		Lee *et al.* 2013
Paddy straw	500	10	> 60	41		Lee *et al.* 2013
PKS	500	10	> 60	32.2		Lee *et al.* 2013
Wood stem	500	10	> 60	22.3		Lee *et al.* 2013
Wood bark	500	10	> 60	31.9		Lee *et al.* 2013
Ulva sp.	600	30	40	30.5		Mondal *et al.* 2024
Asparagopsis	600	30	40	40		Mondal *et al.* 2024
Oedogonium	600	30	40	28.2		Mondal *et al.* 2024
Kappaphycus alvarezii	600	30	40	41.6		Mondal *et al.* 2024
Eucheuma denticulatum	600	30	40	47.0		Mondal *et al.* 2024
Sargassum sp.	400	7	60	n/a	Vacuum	Roche *et al.* 2023
Ulva expansa	500 to 900	5	120	18.9 to 42.7	Oxidation at 200 to 300 °C with 150 min residence time	This work
Sargassum sp.	500 to 900	5	120	26.4 to 39	Oxidation at 200 to 300 °C with 150 min residence time	This work

Although terrestrial feedstocks such as wood stem or corn straw have been traditionally utilized as biochar sources, marine biomass also demonstrates comparable yields, often ranging from ~20% to above 40%, depending on the specific species and thermal processing conditions. Additional motivation for utilization of aquatic macroalgae includes their rapid growth, diverse composition, widespread availability, and limited need for arable land or fertilizers. Notably, macroalgal species provide ecological benefits, such as serving as habitats for aquatic life and buffering ocean acidification and warming (Duarte *et al.* 2021). Compared to land plants, macroalgae contain similarly large amounts of carbohydrates, albeit with comparatively more diverse composition (Zadeh *et al.* 2020; Singh *et al.* 2021; Zhao *et al.* 2022). Among macroalgae, *Ulva expansa* (ulva) and *Sargassum* sp. (sargassum) have demonstrated potential in many bioproduct applications, including in biochars (Atugoda *et al.* 2021; Roche *et al.* 2023; Mondal *et al.* 2024; Shoaib *et al.* 2024), yet their distinctly different compositions warrant further examination of how they could affect biochar structure and mechanical properties. Aiming to contribute to this knowledge gap, in this study, the authors investigate the effects of high- and low-temperature pyrolysis (500 to 900 °C) on the structure and mechanical properties of biochars derived from ulva and sargassum. This study aims to understand how pyrolysis parameters and algal composition influence carbon yield, crystallinity, functional groups, and mechanical performance, contributing to the development of tailored biochars for environmental and industrial applications.

EXPERIMENTAL

Materials

Raw ulva (a green macroalga) and sargassum (a brown macroalga) biomass (imaged in Fig. 1a,b) were kindly provided from the Pacific Northwest National Laboratory (Sequim, WA, USA) and Algas Organics (St. Lucia). Their relative composition is reported in Table 2. Ash content was measured gravimetrically following combustion at 550 °C in a muffle furnace. Moisture was determined gravimetrically in a vacuum oven. Total nitrogen was analyzed using a combustion instrument based on the Dumas principle; protein content was then estimated by applying a conversion factor of 6.25 (Grandgeorge *et al.* 2024). Lipid content was quantified by hydrolysis and subsequent ether extraction, and the carbohydrate fraction was calculated by difference (Buckee 1994). In preparation for treatment, blades of sargassum were removed from the stem, triple washed with deionized water, and subsequently dehydrated by heating in 80 °C for 24 h. Both species were ground using an electric grinder before speed milling (DAC 330-100 PRO; FlakTek, Landrum, SC, USA) at 2500 rpm for 1 min. Milled material was passed through a sieve tower and powders that passed through a 150-µm sieve were used in subsequent experiments.

Table 2. Relative Amounts of Macromolecules Present in Each Alga

Biomass Type	Carbohydrates	Proteins	Lipids	Ash	Moisture
Ulva	58.6%	5.30%	0.6%	23.5%	12%
Sargassum	65.5%	5.45%	< 0.5%	16.8%	12.3%

Methods

Thermal treatment

Thermogravimetric analysis (TGA) was conducted using a Discovery TGA 550 (TA Instruments, New Castle, DE, USA) device. Samples of 10 ± 4 mg of each material were loaded into alumina crucibles and subjected to two heating regiments: heated from room temperature (RT) to 900 °C in air (Fig. 1d), and in nitrogen (Fig. 1e). These experiments were conducted with a heating rate of 5 °C/min and with a gas flow rate of 25 µL/min. The TGA was also used to determine algal ash content. The raw algal powders (~15 mg) were loaded into platinum crucibles and heated in air to 105 °C at 10 °C/min and held for 30 min. It is this resulting mass that corresponds to the initial sample dry mass, devoid of ambient moisture. Samples were then ramped in air at 10 °C/min to 575 °C and held for 3 h. The final mass was compared to the initial mass to determine the ash content.

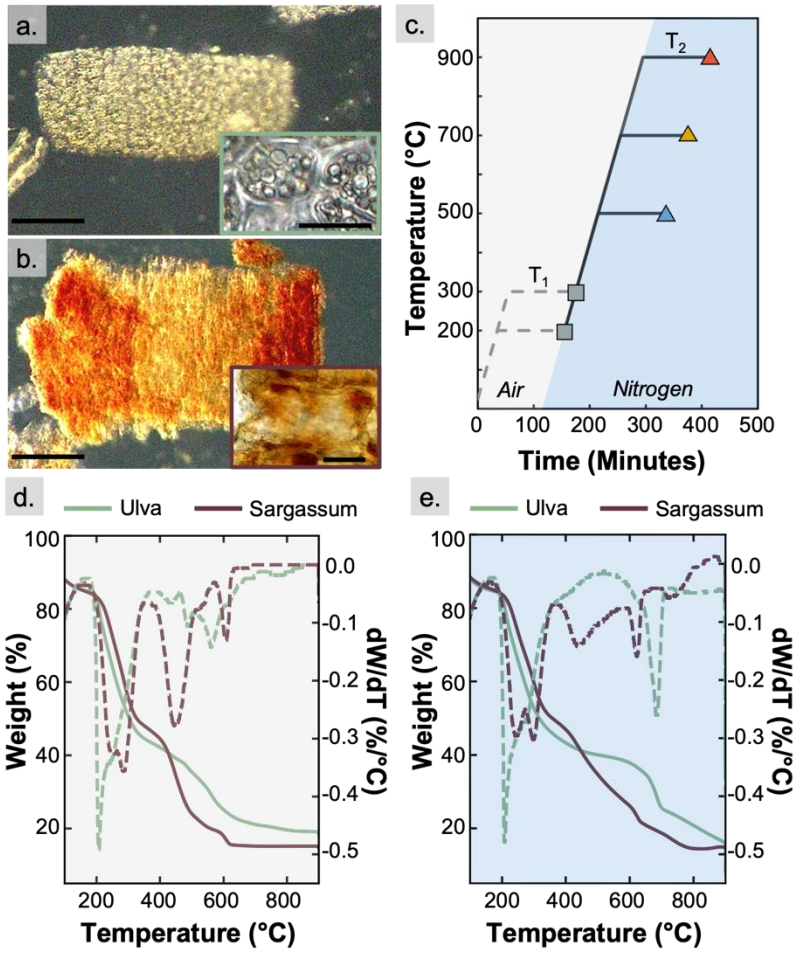

Fig. 1. Optical microscopy of algal tissue flakes (scale bar = 100 µm) with insets of individual cells (inset scale bar = 20 µm) for (a) ulva and (b) sargassum; (c) Schematic outlining pyrolysis heating conditions; TGA/DTG curves from thermal analysis tests conducted in (d) air and (e) nitrogen

Pyrolysis of both biomasses was performed in a tube furnace (TF1 12/60/300, Carbolite Gero, Hope Valley, United Kingdom). Approximately 1.00 ± 0.25 g of each powdered sample was loaded in alumina crucibles and inserted into the furnace. Experiments began with oxidation under an air flow of 65 sccm with an initial ramp from RT to T_1 (set at 200 or 300 °C) at a heating rate of 5 °C/min, and then held for 2.5 h. After

the T_1 hold, the gas was switched to nitrogen (gas flow of 65 sccm) and the temperature was increased to T_2 (set at 500, 700, or 900 °C) at a heating rate of 5 °C/min and held for 2 h. The heating conditions are schematically depicted in Fig. 1c, and the individual pyrolysis experiments are listed in Table 3. Samples will be referenced using shorthand notation such as $X/A_y/N_z$, where "X" will be either S for sargassum or U for ulva, "y" will be the T_1 temperature (200 or 300 °C) of the first heating conducted in air (oxidation process), and "z" will be the T_2 temperature (500, 700 or 900 °C) of the second heating conducted in nitrogen (pyrolysis process). Samples that were subjected only to the initial oxidation step (U/A_{200}, U/A_{300}, S/A_{200}, and S/A_{300}) will be referred to as intermediates in the text.

Chemical and structural analyses

To characterize both algae and resulting biochars, X-ray diffraction (XRD) was conducted using a D8 Advance XRD (Bruker, Billerica, MA, USA) with Cu Kα X-ray radiation (wavelength of 1.5406 Å) on powdered samples. The X-ray was powered to 40 kV and 40 mA, and the diffraction pattern was collected from 10°to 90° 2θ with a step size of 0.02° and a collection of 0.07 s/step.

A Thermo Scientific DXR2 confocal Raman microscope (Waltham, MA, USA), equipped with 785 and 532 nm laser sources, was utilized to collect Raman spectra from the powders before and after heat treatment. Acquisition parameters included a 10x objective lens, 50 μm aperture, 8 to 28 mW laser power, and a total exposure time of 40 s. In post-processing, a linear baseline correction was applied between 1000 and 1800 cm^{-1}, and the resulting intensity ratios of the D (~1344 cm^{-1}) to G (~1579 cm^{-1}) peaks were calculated before peak intensity was normalized to the D peak.

X-ray photoelectron spectroscopy (XPS) spectra of raw ulva, raw sargassum, $U/A_{300}/N_{900}$, and $S/A_{300}/N_{900}$ were measured on an Axis-Ultra DLD spectrometer (Kratos Analytical, Manchester, UK). This instrument has a monochromatized Al Kα X-ray and a low energy electron flood gun for charge neutralization. X-ray spot size for these acquisitions was on the order of 700 x 300 μm. Pressure in the analytical chamber during spectral acquisition was less than 5 x 10^{-9} Torr. Pass energy for survey and detailed spectra (composition) was 80 eV. Pass energy for the high-resolution spectra was 20 eV. The take-off angle (the angle between the sample normal and the input axis of the energy analyzer) was 0^o (0^o take-off angle ~ 100 Å sampling depth). The Kratos Vision2 software (Kratos Analytical, Manchester, UK) was used to determine peak areas and to calculate the elemental compositions from peak areas. CasaXPS was used to peak fit the high-resolution spectra. For the high-resolution spectra, a Shirley background was used, and all binding energies were referenced to the C ls C-C bonds at 285.0 eV.

X-Ray Fluorescence (XRF) measurements were conducted using a Bruker M4 Tornado (Bruker, Billerica, MA, USA) with a Rh anode tube on powdered samples.

Morphological and mechanical analyses

Intermediate and pyrolyzed samples were characterized for their reduced modulus through nanoindentation (FT-MTA03, FemtoTools, Zurich, Switzerland). Powdered samples were first mounted on stubs with super glue. After at least 12 h of setting, the surface was sanded to 2000 grit to ensure a sufficiently flat probing surface. Indentation was conducted using a Berkovich tip for all samples using a force-controlled test to 200 mN where load and unload rate were set to 100 mN/s and the maximum probing depth was 1.5 μm. The reduced modulus of elasticity, E_r, was determined using the unloading portion

of the force *vs.* displacement curves and fitting the slope to the Oliver Pharr contact model. Samples were probed at different points (n = 5 per sample), and statistical analysis was performed using a pairwise Welch's t-test.

For biochar imaging, non-conductive samples were sputter coated with a gold-palladium alloy and imaged with a scanning electron microscope (SEM) (JSM-6010 Plus, JEOL, Peabody, MA, USA) with a voltage of 10 kV. Localized elemental analysis was conducted through energy dispersive spectroscopy (EDS), in which the voltage was increased to 15 kV, respectively, to increase the signal intensity for a better EDS reading. Subsequent data processing removed the gold and palladium content as these coated materials were not expected in any measured samples.

RESULTS AND DISCUSSION

Comparing the raw algal powders, optical microscopy images (Fig. 1a) show that ulva cells were rounded, ~21 μm in diameter, while sargassum cells are more elongated, with sizes of ~27 x 63 μm. Table 2 provides the compositional breakdown of both algae, revealing that carbohydrates were the predominant organic component. Together with inorganics (ash), carbohydrates constituted the majority of the biomass weight. Protein and lipid contents, although present, were relatively minor in comparison. Ash measurements indicate that ulva and sargassum contained 24.9% and 16.6% ash, respectively. Notably, ulva had a higher carbohydrate-to-ash ratio than sargassum. In addition to these differences, there were distinctions in carbohydrate types; while both algae contained cellulose (Doh and Whiteside 2020; Li *et al.* 2023), the ulva was rich in ulvan, whereas the sargassum contained fucoidans and alginic acid (commonly present as alginate).

Thermal Treatment

The TGA was performed on raw ulva and sargassum samples from RT-900 °C in air and in nitrogen to characterize thermal degradation and guide the selection of pyrolysis temperatures. The resulting TGA curves (Fig. 1d, 1e) reveal three distinct degradation stages for both species. Stage I (RT to ~200 °C) was marked by mass loss attributed to free water and residual moisture. Stage II (200 to 350 °C) involves the decomposition of cellulose and other carbohydrates. Ulva and sargassum exhibited significant mass losses of 38.0% and 32.2%, respectively in that stage. In ulva, the sharp peak in the derivative (DTG, dashed line) at about 200 °C corresponds to the degradation of ulvan (Alves *et al.* 2010). Both species displayed a shoulder at 250 °C, likely related to cellulose, a shared component for both macroalgae (Alvarado Flores *et al.* 2022). Around 270 °C, sargassum showed an additional peak attributed to alginate and fucoidans, common components of brown algae (Bilba *et al.* 2023). The higher degradation temperature of these components in sargassum could be attributed to their higher molecular weights and compositional differences inducing higher thermal stability compared to carbohydrates that decompose at lower temperatures. Stage III (> 350 °C) accounts for 31.9% mass loss in ulva and 39.5% in sargassum. A DTG peak near 450 °C was observed in both species, commonly associated with the degradation of proteins or aromatic compounds (*e.g.*, polyphenols, chlorophyll, vitamins) (Wang *et al.* 2021; Bilba *et al.* 2023). The greater mass loss in sargassum at this stage indicates a higher overall fraction of these high-temperature constituents. While proteins generally degrade into volatile products rather than solid char (Debono and Villot 2015; Leng *et al.* 2020), aromatic compounds contribute to carbon retention due to their

pre-existing stable ring structures (Kabakcı and Hacıbektaşoğlu 2017). Above 600 °C, smaller peaks were observed in both macroalgae, corresponding to salt decomposition events (Alves *et al.* 2010; Wang *et al.* 2021).

Overall, the sargassum was slightly more thermally stable than the ulva between 200 and 400 °C. For instance, both samples lost ~17% mass by 200 °C, whereas at 300 °C the mass losses were 40.6% for sargassum and 47.5% for ulva. These differences may reflect compositional and structural variations, including the distribution of cellulose, alginate, fucoidans, and ulvans in the cell walls. Above 500 °C, ulva became more thermally stable than sargassum, with the greatest difference observed at 507 °C (13.4%). Specifically, the difference in mass loss was 11.5% at 500 °C and 5.9% at 700 °C. The final residues in air after a 2 h hold at 900 °C, were 17.9% for ulva and 14.8% for sargassum, whereas in nitrogen they were 8.2% and 14.6%, respectively. From these profiles, two temperatures (200 and 300 °C) were selected for oxidative stabilization, given the notable differences in carbohydrate degradation. Subsequent pyrolysis runs were conducted at 500, 700, and 900 °C to investigate how varying amounts of organic content affects the final biochar.

Table 3 summarizes the heat treatment conditions and mass loss data. Each biomass underwent an oxidation step from RT to T_1 (200 or 300 °C) in air. To assess this oxidative stabilization, intermediate samples were removed immediately after this step and characterized. The final masses of U/A_{200} and S/A_{200} were 75.9% and 75.5%, respectively, while U/A_{300} and S/A_{300} were 42.7% and 43.5%. In both cases, the similar mass losses for the two species indicate that oxidation at 200 and 300 °C induced comparable changes in ulva and sargassum. Clearly, oxidation at 200 °C retained more organic content than oxidation at 300 °C, where more extensive decomposition occurred.

Table 3. Summary of Pyrolysis Conditions, Measured Yield and Raman-measured ID/IG Peak Ratios

Biomass Type	T_1 (°C)	T_2 (°C)	Final Weight (%)	I_D/I_G
Ulva	200	-	75.9	-
		500	42.7	0.920
		700	31.3	1.016
		900	26.9	0.992
	300	-	42.7	-
		500	37.4	0.932
		700	19.2	1.118
		900	18.9	1.039
Sargassum	200	-	75.5	-
		500	39.0	1.000
		700	31.1	1.056
		900	29.0	0.973
	300	-	43.5	-
		500	34.2	0.816
		700	27.3	1.069
		900	26.4	0.975

To elucidate the impact of oxidative stabilization, the authors compared final residues at each pyrolysis temperature (T_2) for samples processed in nitrogen alone *versus* those first oxidized. Note that the nitrogen-only residues for pyrolysis temperatures other than 900 °C discussed in this section were derived from TGA runs without a 2 h isotherm, whereas pyrolysis runs with prior oxidation (*e.g.*, U/A_{200}/N_{500}) included a 2 h hold at T_2.

For ulva in pure nitrogen at 500 °C, the residue was 40%, whereas U/A_{200}/N_{500} and U/A_{300}/N_{500} yielded 42.7% and 37.4%, respectively. The slightly higher residue after oxidation at 200 °C (+2.7%) suggests the formation of a higher amount of thermally stable intermediate compounds that subsequently transform to carbon. In contrast, oxidation at 300 °C led to a lower yield than the no-oxidation case (37.4% *vs.* 40%), indicating that further organic decomposition occurred under these conditions. Sargassum exhibited a similar trend overall, but the influence of the 200 °C oxidation step was more pronounced. The residue increased from 34.6% (in pure nitrogen) to 39% for S/A_{200}/N_{500}, whereas oxidation at 300 °C yielded 34%, which was marginally below the no-oxidation condition. Thus, the 200 °C oxidation step improved the carbon yield by +4.4% relative to no oxidation, whereas oxidation at 300 °C resulted in a −0.6% change. Compositional differences between ulva and sargassum likely underlie these observations. Both algae share cellulose as one of the major carbohydrates, but ulva also contains ulvans, which degrade at ~200 to 250 °C, whereas sargassum contains alginate and fucoidans that degrade near 270 °C. The more substantial carbon retention in sargassum may be attributed to (1) greater amounts of carbohydrates that are stabilized by oxidation and (2) higher fraction of components degrading at 450 to 500 °C, which include aromatics and proteins, of which aromatic compounds are prone to forming stable carbon residues. In ulva, the lower thermal stability of ulvans led to greater losses during oxidation, while the lower fraction of thermally stable organics also contributed to the lower carbon yield compared to sargassum. In both species, oxidation at 300 °C ultimately proved detrimental for carbon yield, while oxidation at 200 °C is beneficial.

A similar pattern emerged at 700 °C. For ulva in pure nitrogen, the residue was 25.5%, whereas U/A_{200}/N_{700} yielded 31.3% (+5.8%) and U/A_{300}/N_{700} yielded 19.2% (−6.3%). Sargassum in pure nitrogen at 700 °C showed 18.7% residue, which increased to 31.1% (+12.4%) for S/A_{200}/N_{700} and 27.3% (+8.6%) for S/A_{300}/N_{700}. These results reinforce the greater benefit of 200 °C oxidation in forming thermally stable intermediates, particularly in sargassum, where alginate and fucoidans appeared more effectively stabilized at lower oxidation temperatures. In addition, sargassum's potentially greater aromatic content may further enhance carbon formation.

A similar trend was observed at 900 °C, where the final yield increased substantially following oxidative pretreatment. For ulva in pure nitrogen, the residue at 900 °C was 8.2%, whereas U/A_{200}/N_{900} and U/A_{300}/N_{900} yielded 26.9% and 18.9%, respectively. These values translate to solid mass increases of +18.7% and +10.7% over the no-oxidation condition. Sargassum also benefited markedly from oxidation. The nitrogen-only residue of 14.6% rose to 29% (+14.4%) with 200 °C oxidation and 26.4% (+11.8%) with 300 °C oxidation. It was noted that pyrolysis at 900 °C was the only condition for which the ulva biochars saw more benefit from the 200 °C oxidation process than sargassum. These results underscore the effectiveness of the oxidative stabilization step at generating thermally stable intermediate compounds that enhance carbon retention, even at higher pyrolysis temperatures. The effects were more pronounced overall for oxidation at 200 °C.

The final solid residue after each pyrolysis experiment reflected the biochar yield. Increasing both T_1 (oxidation) and T_2 (pyrolysis) generally reduced final yield for both biomasses. However, the change from A_{300}/N_{700} to A_{300}/N_{900} was smaller, suggesting that most organic components had decomposed by 700 °C and thus, a similar amount of carbon could be formed in those cases. As previously discussed, comparing biochars from A_{200} and A_{300} oxidation steps also showed that higher T_1 lowered the overall yield. This

difference was maximized in ulva, where U/A_{200}/$N_{700–900}$ exhibited 8.0 to 12.1% higher residual mass than U/A_{300}/$N_{700–900}$. Unlike the intermediate products, the final biochars showed marked variability in the mass loss between the two species, as discussed previously. For example, at 500 °C, U/A_{200}/N_{500} retained 42.7% mass, while S/A_{200}/N_{500} retained 39.0%. Conversely, at 700 °C under A_{300} conditions, ulva yielded only 19.2% compared to 27.3% for sargassum. These trends reflect underlying compositional differences between the species.

Comparisons between the final pyrolysis yields and the ash contents listed in Table 2 indicate that the solid residue was primarily composed of ash, with the remaining balance being carbon. For instance, U/A_{200}/N_{500} retained 17.8% carbon, which decreased to 6.4% for U/A_{200}/N_{700} and 2.0% for U/A_{200}/N_{900}. When the oxidation temperature was raised to 300 °C, carbon retention diminished, with only the U/A_{300}/N_{500} sample yielding a detectable 12.5% carbon. Sargassum showed a similar pattern of decreasing carbon content with increasing pyrolysis temperature yet exhibited comparatively higher retention at lower temperatures. For example, S/A_{200}/N_{500} retained 22.6% carbon, dropping to 14.7% at 700 °C (S/A_{200}/N_{700}) and 12.6% at 900 °C (S/A_{200}/N_{900}). These data highlight the combined effects of oxidation protocol and pyrolysis temperature on carbon preservation: oxidation at 200 °C generated more thermally stable precursors than at 300 °C, and higher pyrolysis temperatures generally reduced organic content and thus carbon yield for both species. Moreover, the overall yields reported in this study (18.9 to 42.7% for ulva, 26.4 to 39% for sargassum) fell within the typical range (22 to 50%) documented for agricultural residues (*e.g.*, rice straw, corn straw, garden waste) and woody feedstocks, as summarized in Table 1. Despite having a distinctly different chemical makeup relative to lignocellulosic materials, macroalgae can exhibit comparable final yields. Recent work on other macroalgae (*e.g.*, *Asparagopsis*, *Kappaphycus alvarezii*) similarly shows yield ranges of 28.2 to 47.0%, underscoring macroalgae's potential as an alternative feedstock for biochar production. The subsequent sections further examine how these factors influence the carbon structure and overall composition of the final biochars.

Chemical and Structural Analyses

To analyze the amount and structure of the produced carbon in the algal biochars, Raman and XPS spectroscopies were used. Figure 2 presents the Raman spectra of all pyrolyzed samples of ulva and sargassum, obtained after oxidation at T_1 = 200 °C (Fig. 2a, 2b) and 300 °C (Fig. 2c, 2d). The collected spectra confirm the presence of carbon in all pyrolyzed biochars, indicated by the sole and prominent D and G band peaks associated with disordered and graphitic carbon, respectively (McDonald-Wharry *et al.* 2013). Therefore, these spectra together with the ash content measurements confirm that the pyrolyzed biochars derived from ulva and sargassum were composed of ash and carbon. The intensity ratio of the D band with respect to the G band (I_D/I_G) is commonly used to indicate the level of morphological disorder in carbon materials, where higher values indicate a more disordered or defect-dominant system and lower values conversely indicate a more ordered or graphitic system (McDonald-Wharry *et al.* 2013). In Table 3, the calculated I_D/I_G ratios for all biochars are presented. It is worth mentioning that the largest value, or most disordered carbon, occurred at A_{200}/N_{700} for both biomasses with the highest overall value occurring in ulva (1.118). The lowest, or most ordered carbon, occurred at T_2 = 500 °C for most samples with the lowest overall measured at 0.816 for S/A_{300}/N_{500}. In both biochars and at both oxidation temperatures, the I_D/I_G ratio increased from 500 to 700 °C followed by a decrease from 700 to 900 °C.

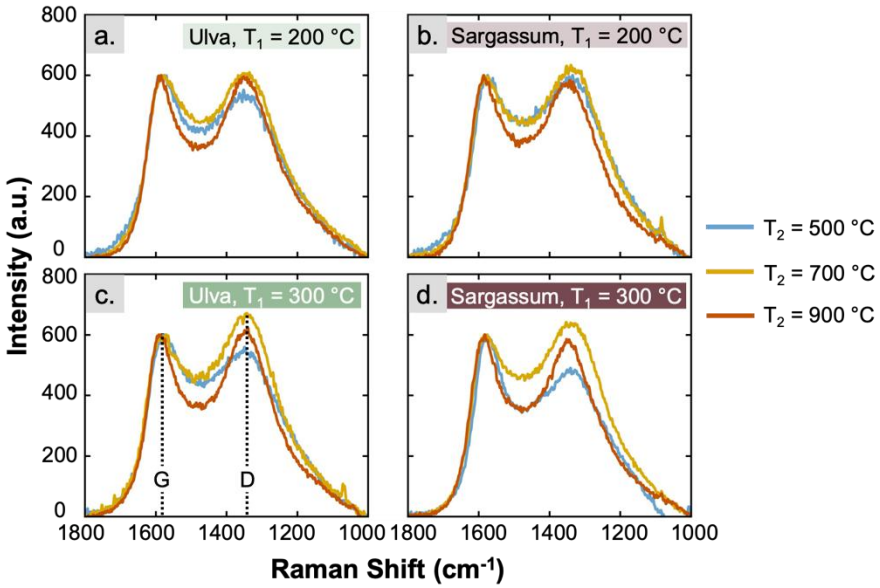

Fig. 2. Raman spectra of pyrolyzed (a, c) ulva and (b, d) sargassum, comparing oxidation at (a, b) 200 °C or (c, d) 300 °C followed by pyrolysis at 500, 700, and 900 °C

The surface chemistry of both raw and pyrolyzed material was investigated using XPS to corroborate the presence of carbon observed in Raman spectroscopy while also providing further insights to carbon hybridization states. Ulva and sargassum raw biomass before any heat treatment, as well as the A_{300}/N_{900} samples were characterized with XPS. Figure 3a presents the C 1s spectra of the raw algal biomasses and the A_{300}/N_{900} biochars with peak deconvolution, while Fig. 3b presents the derived peak area with the peak location noted for each sample. As reported in literature, peak deconvolution attributes the observed peak at ~285 eV to C-C bonding, followed by another peak at ~286 eV correlated to C-O bonding, and finally the highest energy peak at ~288 eV representing C=O bonds (Wu *et al.* 2021). Notably, the deconvolution of the C-C peak and peak area analysis indicated that more carbon participating in graphitic or amorphous structures was present in $U/A_{300}/N_{900}$ compared to $S/A_{300}/N_{900}$. In contrast, sargassum both before and after pyrolysis had more carbon functional groups present, as indicated by the higher relative amounts of C-O and C=O peaks. Furthermore, the pyrolysis of ulva appears to induce a peak shift of the C-C peak from 285.0 to 284.7 eV, whereas in sargassum this peak shifted closer to 284.2 eV. The differences in C-C peak locations between $U/A_{300}/N_{900}$ and $S/A_{300}/N_{900}$ is attributed to the relative amounts of sp^3 and sp^2 hybridized carbon, where peaks closer to 285.0 eV are related to sp^3 hybridization and peaks closer to 284.2 eV are related to sp^2 hybridization (Kozakov *et al.* 2021). While the exact relative amounts of sp^3 and sp^2 hybridization are not determined in the current study, the results suggest the presence of amorphous carbon (mix of sp^2 and sp^3) in both cases with a more sp^2 carbon in sargassum biochar and more sp^3 carbon in ulva biochar.

Figure 3b shows the pyrolysis of ulva caused a relative increase in C-C bonds, while in sargassum there was a striking decrease. Conversely, the lower amount of C-O bonds in ulva is further reduced after pyrolysis, with the low amount of C=O bonds remaining at the same levels. On the other hand, the C-O bonds in sargassum saw a small decrease while the C=O bonds drastically increased after pyrolysis. The changes in peak area overall

suggest that sargassum biochars contained more functional groups in the final biochar material while ulva biochars had more saturated C-C bonds.

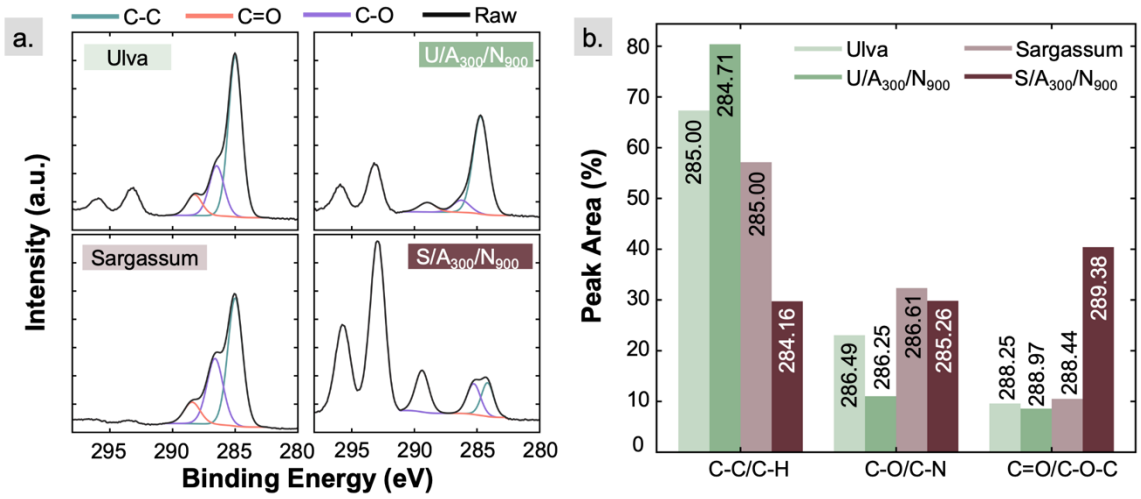

Fig. 3. (a) High resolution C 1s XPS data with peak deconvolution and (b) peak area percentages labelled with binding energy of each peak, for the raw biomass, U/A300/N900 and S/A300/N900

The elemental analysis also provided by XPS is presented in Table 4. Both raw biomasses were composed largely of carbon and oxygen with very low amounts of inorganics such as sodium and magnesium. As a result of pyrolysis and the thermal decomposition of organics, both U/A300/N900 and S/A300/N900 biochars had lower relative amounts of carbon and higher relative amounts of oxygen with respect to the raw biomass. For the same reason, the biochars showed a relatively increased amount of previously low-content or trace elements. For example, the U/A300/N900 sample contained 7.2 at% sulfur, 8.1 at% sodium, and 2.8 at% potassium. The S/A300/N900 sample contained 4.7 at% sodium, 3 at% magnesium, and 13.8 at% potassium. It is worth clarifying that the reported amounts of inorganics were relative in each analyzed sample, meaning there was no actual increase in their amounts, but rather there was a large decrease in the amount of carbon due to the decomposition of organics.

To complement our XPS findings with a bulk inorganic perspective, XRF analyses were conducted for selected raw and pyrolyzed samples. Because the used Rh-source XRF cannot detect elements lighter than sodium (*i.e.*, carbon, nitrogen, and oxygen), it only measures heavier elements ($Z \geq 11$), which in this case primarily represent the inorganic components present in the biomass. In raw ulva, sulfur (36.5 wt%), potassium (27.2 wt%), chlorine (25.6 wt%), and magnesium (7.1 wt%) were detected. After pyrolysis at 900 °C with a 300 °C oxidation step, sulfur (42.0 wt%) and magnesium (25.1 wt%) were relatively increased, while potassium (16.8 wt%) and sodium (10.9 wt%) were also detected. In Sargassum, the raw material was high in calcium (54.2 wt%), sulfur (19.1 wt%), and potassium (18.9 wt%), whereas S/A300/N900 contained more balanced levels of calcium (31.9 wt%), sulfur (31.7 wt%), potassium (16.4 wt%), and magnesium (10.6 wt%). These shifts underscore how high-temperature treatment can transform or concentrate inorganic salts and minerals as the organic fraction decomposes. By focusing on bulk inorganics, XRF thus provides a useful complement to the surface-sensitive XPS data, offering a more comprehensive view of each sample's overall elemental composition.

The presence of inorganics was supported further through analysis of the higher energy peaks in the pyrolyzed samples. The two peaks at ~293.4 eV and ~296.0 eV, which were present in all but the raw sargassum spectra, were associated with the potassium $2p^{3/2}$ and $2p^{1/2}$ peaks, respectively. Additionally, the smaller individual peak that forms around 289.4 eV in the $U/A_{300}/N_{900}$ and $S/A_{300}/N_{900}$ was related to the presence of carbonated salts (Gorham 2012). Previously discussed ash tests confirmed the presence of inorganics, and the XPS data corroborate that while also revealing the formation of carbonates, a phenomenon that is known to occur in biochar production from pyrolysis (Singh *et al.* 2017). The presence of salts as a function of heating treatment is explored further with XRD and EDS discussed in the following sections.

Table 4. Breakdown of Atomic Percentages in Raw and Pyrolyzed Samples at A_{300}/N_{900} as Measured from XPS Wide Scans

	Atomic (%)			
Element	Sargassum	$S/A_{300}/N_{900}$	Ulva	$U/A_{300}/N_{900}$
C	74.2	22.9	61.8	34.3
N	1.8		2.6	
O	23.4	47.8	25.6	41.3
Na		4.7	1.4	8.1
Na^-	trace			
Mg	trace	3.0	1.8	6.3
P		1.3		
S	0.6	0.9	4.3	7.2
Cl		3.6	0.7	
K		13.8	1.9	2.8
Ca		2.0		

In the context of biochar, the amorphous and crystalline phases present in XRD spectra provide useful information regarding the presence of carbon and salts/inorganics. In Figs. 4a and 4d, the XRD spectra of all raw, intermediate, and pyrolyzed samples are presented. First, regarding sargassum, the raw spectra exhibited a broad peak located at ~22.8° 2θ, which can be associated with semicrystalline cellulose or alginate (Kim *et al.* 2013; Bhagyaraj and Krupa 2020; Thabet *et al.* 2024). This peak remains intact in the intermediate S/A_{200} sample, while it was entirely diminished in the intermediate S/A_{300} sample, indicating that the cellulose and/or alginate components were at least partially preserved upon oxidation at 200 °C but entirely combusted by 300 °C, which is in agreement with the TGA results previously discussed. This broad peak is present in the raw ulva as well but is much less pronounced as other crystalline materials dominate the ulva spectra even in its raw form.

Another small peak at 30° is attributed to calcite (Singh *et al.* 2017; Zhao *et al.* 2022), though it was not detected above N_{500} despite literature indicating that calcite begins to degrade after ~600 °C (Li *et al.* 2017). This peak is also associated with quartz (Singh *et al.* 2010), so it was likely a convolution of multiple inorganic crystals. For both ulva and sargassum, sharp peaks began to form and dominate the spectra as a result of full pyrolysis ($A_{200\text{-}300}/N_{500}$), signaling that the present crystalline salts in both biochars were dominant compared to any remaining crystalline carbohydrates (Kim *et al.* 2013) or pure carbon (Manoj and Kunjomana 2012; Singh *et al.* 2017). The presence of any significant amount of crystalline carbon is also unlikely in all biochars, as the (002) band at 25.5° and (10) band at 42.3° were not present in all spectra (Manoj and Kunjomana 2012). Combined with

XPS observations of carbonated salts at ~290 eV, these new sharp peaks in the XRD patterns above 20° strongly indicate carbonate formation within the biochars. Such carbonates arise from the reaction of inorganic species, originally present in the raw algae, that survive or form under the pyrolysis conditions. Consequently, the XRD results predominantly capture the evolution of inorganic mineral phases (salts and carbonates), demonstrating that they became increasingly significant contributors to the final biochar structure as organic constituents were decomposed at higher temperatures.

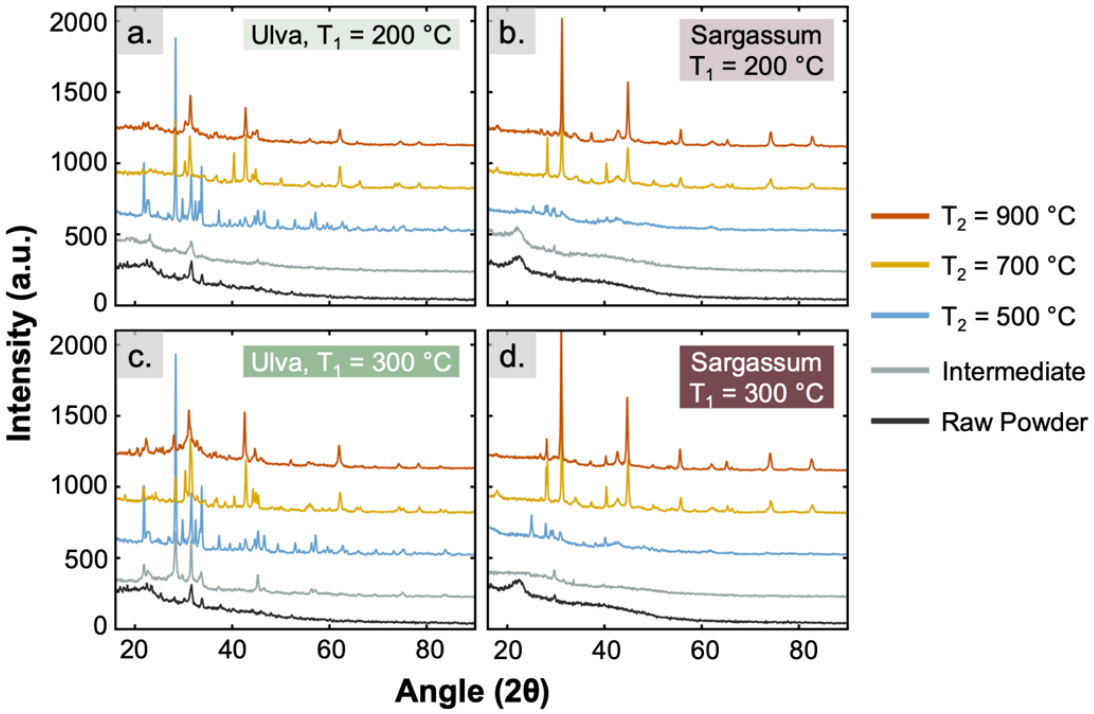

Fig. 4. XRD spectra of (a, c) ulva and (b, d) sargassum biomass and biochars as a function of heating conditions

Morphological and Mechanical Analyses

Nanoindentation was employed to measure the reduced modulus of the intermediate and biochar products, as presented in Fig. 5a for ulva and Fig. 5b for sargassum. In both biomasses, resultant biochars possessed distinctly different mechanical properties as a result of varied heating conditions. U/A_{200} samples were able to attain reduced modulus of ~3 GPa and U/A_{300} samples were enhanced further to reach up to ~7 GPa. Sargassum biochar reached even further enhancement, with S/A_{200} and S/A_{300} samples reaching up to ~5 and ~8 GPa, respectively. The range of observed reduced moduli produced from ulva and sargassum biomass was in agreement with literature reported biochars from woody biomass (3.3 to 7.3 GPa) (Das *et al.* 2016; Wallace *et al.* 2019).

Despite these overall similarities, ulva and sargassum biochars exhibited notable differences in how oxidation temperature influenced their mechanical behavior. In ulva, it is apparent that changes induced during the oxidation at 200 °C (U/A_{200} samples) dominated the resulting mechanical properties, as all fully pyrolyzed U/A_{200} samples had statistically similar reduced moduli. Mass loss data (Table 3) reveal that the U/A_{200} samples retained more carbon than the U/A_{300} samples after oxidative stabilization – likely due to

the stabilization of carbohydrates – thus leaving more carbon available for subsequent pyrolysis and incorporation into the biochar. The nanoindentation data suggest that this preserved carbon dominated the mechanical properties. Conversely, the U/A_{300} samples exhibited properties more heavily influenced by salt or inorganic content, as they contained significantly less carbon than U/A_{200} samples. Therefore, the final pyrolysis temperature affected the mechanical properties more significantly for the U/A_{300} samples. The U/A_{300}/N_{500} biochar showed a ~40% reduction from the U/A_{300} intermediate product, followed by another ~35% decrease when the temperature increased to 700 °C. Above 700 °C, degradation of salts (Li *et al.* 2017; Bedoya-Henao *et al.* 2025) and formation of carbonates, corroborated by XPS (Fig. 3a) and XRD (Fig. 4a), likely play a role. It is worth mentioning that raising the temperature from 700 to 900 °C then causes an unexpected ~78% increase in reduced modulus for U/A_{300}/N_{900}. This may result from a combination of mineral transformations (*e.g.*, salt decomposition, carbonate formation) and changes in the carbon structure as indicated by the I_D/I_G ratios in Raman spectroscopy.

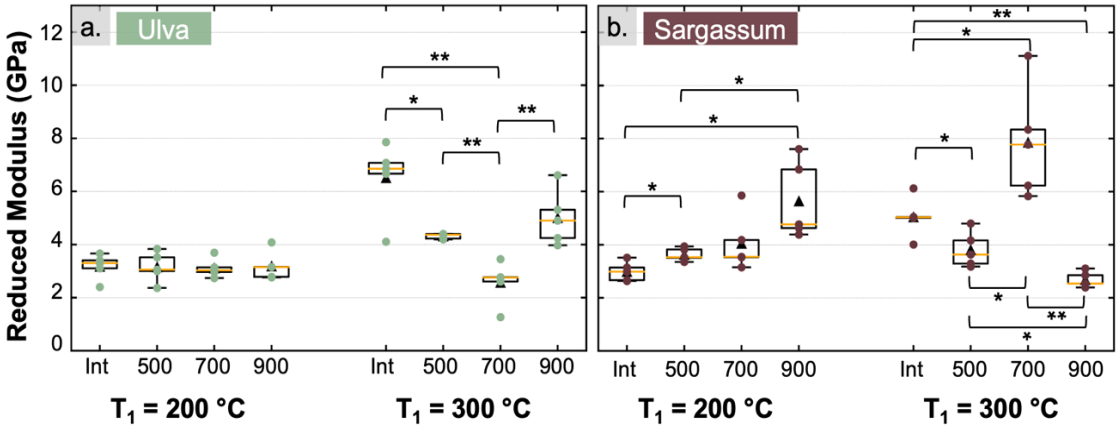

Fig. 5. Reduced modulus in (a) ulva and (b) sargassum, grouped by T_1 (*p < 0.05 and **p < 0.01)

Although sargassum biochars followed some similar trends, they demonstrated distinct pathways for mechanical-property development. The S/A_{200} intermediate had a reduced modulus comparable to the U/A_{200} intermediate; however, the fully pyrolyzed S/A_{200} samples exhibited incremental increases from 500 to 900 °C. In contrast, the S/A_{300} samples had a more irregular trajectory with increasing final pyrolysis temperature.

There was a ~26% decrease from the S/A_{300} intermediate to S/A_{300}/N_{500}, followed by a ~210% increase at 700 °C (S/A_{300}/N_{700}) and then a ~65% drop at 900 °C (S/A_{300}/N_{900}). As indicated by the previous results, sargassum retained a higher fraction of carbon overall – partly attributable to its carbohydrates (alginate, fucoidans) and higher amounts of aromatics and/or proteins – and that carbon as suggested by XPS had a larger proportion of sp^2-hybridized components. However, pyrolysis facilitates formation and, to some extent, degradation of various salts and carbonates, influencing mechanical properties in complex ways. The measured variability in reduced modulus likely reflects concurrent mechanisms, such as carbohydrate oxidation and stabilization of intermediate compounds, combustion, and salt/carbonate decomposition. Ultimately, these results highlight how algae-derived biochars can exhibit a wide range of mechanical properties governed by (a) inherent compositional differences between ulva and sargassum, and (b) the combined effects of oxidation and pyrolysis temperature. The presence of more thermally stable

carbohydrates (and possibly higher aromatic fractions in sargassum) influences carbon retention and modulates mechanical behavior, while inorganic and carbonate phases can further enhance or diminish stiffness depending on their formation and decomposition pathways.

The SEM analysis of the raw and pyrolyzed materials was conducted to observe microstructural changes resulting from the pyrolysis treatments. Representative SEM images of the raw and A_{300}/N_{900} biochar are presented in Fig. 6.

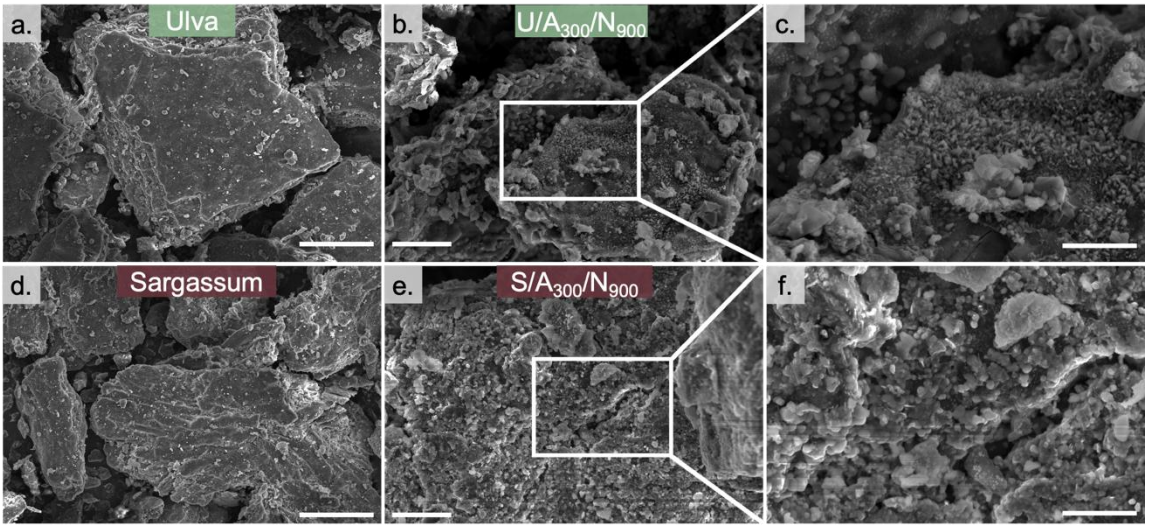

Fig. 6. SEM of raw ulva and sargassum (a,d: scale bar = 50 µm) *versus* pyrolyzed ulva and sargassum (b,e: scale bar = 10 µm) with magnified view of surface components (c,f: scale bar = 5 µm)

Both algal species displayed increased porosity relative to their raw counterparts, although the porosity remained modest compared to woody-biomass-derived biochars (Makowska and Dziosa 2024). This relatively dense morphology is consistent with previous observations in ulva and sargassum biochars (Roche *et al.* 2023; Mondal *et al.* 2024). Comparing the optical microscopy image of raw ulva (Fig. 1a) with the SEM image of $U/A_{300}/N_{900}$ (Fig. 6b, 6c) reveals that ulva biochar retained much of its native, flake-like morphology. Non-conductive samples were sputter-coated for imaging, yet, notably, $S/A_{300}/N_{500}$ did not require sputter-coating, suggesting sufficient electrical conductivity. This observation aligns with Raman data, suggesting that samples with relatively lower I_D/I_G ratios possessed higher graphitic ordering and thus greater electrical conductivity. On the surface of the biochars, various deposited solids were evident – likely salt crystals or carbonates – consistent with the higher inorganic content identified by XPS, XRD, and ash measurements. The EDS elemental analysis supported these observations. For example, in line with our XRF findings, $U/A_{300}/N_{900}$ showed a relative increase of 4.3 wt% potassium, 4.4 wt% sodium, and 3.2 wt% magnesium compared to raw ulva, whereas $S/A_{300}/N_{900}$ showed increases of 4.3 wt% potassium, 2.0 wt% magnesium, and 9.8 wt% calcium relative to raw sargassum. Although these absolute values differ from XRF because the two methods measure different sample depths and use different normalization schemes, the overall trends – increased potassium, magnesium, and other inorganics following pyrolysis – were consistent. These enriched inorganic deposits correlated well with the higher salt and carbonate content indicated by XPS and XRD. Referring to the nanoindentation results,

the prominent surface presence of salts and carbonates helps explain why biochars with higher inorganic content often exhibit more varied stiffness. The overall microstructural changes and compositional differences underscore how oxidative and pyrolysis treatments, along with the inherent compositional makeup of ulva and sargassum, collectively determine biochar properties.

CONCLUSIONS

1. This study demonstrated that *Ulva expansa* (green algae) and *Sargassum* sp. (brown algae) can both serve as viable feedstocks for biochar production through pyrolysis at various temperatures, but their differing organic contents lead to notable variations in carbon yield. Oxidative stabilization at 200 °C generally preserved more thermally stable polymers, thereby increasing the eventual carbon content compared to oxidation at 300 °C. Pyrolysis at 500 °C produced significantly higher yield than 700 and 900 °C independent of oxidation temperature and algal source.
2. The thermogravimetric analysis (TGA) results showed that sargassum exhibited higher thermal stability at moderate temperatures (200 to 400 °C), whereas ulva was more stable above 500 °C. Raman spectroscopy calculated I_D/I_G ratios ranging between 0.82 and 1.12, indicating predominantly disordered (amorphous) carbon in all biochars, with X-ray photoelectron spectroscopy (XPS) suggesting greater sp^2 character in sargassum and relatively more sp^3 in ulva. The XPS also showed that functional groups (C=O, C–O) decreased in ulva but increased in sargassum upon pyrolysis.
3. The X-ray diffraction (XRD), XPS, scanning electron microcopy (SEM), and energy dispersive spectroscopy (EDS) analyses all confirmed the presence of various salts and carbonates in the biochars. The XRD peak intensities varied with different heating conditions, which is correlated to the various salt degradations and carbonate formations. These transformations were most noticeable in the 700 to 900 °C range and influenced the mechanical properties of the final material produced.
4. The SEM images of raw and pyrolyzed samples revealed that both algae-derived biochars were relatively dense compared to lignocellulosic biochars. Deposition of salt crystals and carbonates on the biochar surface was evident, aligning with the higher relative inorganic content measured *via* XPS/EDS.
5. Nanoindentation confirmed that the reduced modulus depended strongly on how much carbon was retained (especially when carbohydrates were stabilized at 200 °C) and on the nature of the inorganic phases. In ulva biochars, oxidation at 200 °C led to relatively consistent mechanical properties due to the preservation of oxidized carbohydrates, which transform to carbon and dominate the biochar mechanical properties. In contrast, ulva biochars oxidized at 300 °C exhibited mechanical properties dominated by the presence and transformations of salts. For sargassum, a broader range of mechanical responses emerged as the oxidation and pyrolysis temperatures varied due to its higher carbon fraction and variable salt transformations, underscoring the feedstock-specific interplay between carbon preservation and inorganic-phase evolution.
6. Overall, the findings highlighted the suitability of macroalgal feedstocks for biochar production, offering a wide range of mechanical properties and surface chemistry that were tunable by oxidation and pyrolysis temperatures. The resulting biochars, rich in

carbon and inorganic phases, may be further optimized for applications spanning soil amendments, filtration media, energy storage, and broader environmental remediation technologies.

ACKNOWLEDGMENTS

This research was partially supported by the U.S. National Science Foundation (NSF) through the UW Molecular Engineering Materials Center (MEM-C), a Materials Research Science and Engineering Center award number (Grant No. DMR-2308979). Part of this work was conducted at the Molecular Analysis Facility, a National Nanotechnology Coordinated Infrastructure (NNCI) site at the University of Washington, which is supported in part by funds from the NSF (awards NNCI-2025489, NNCI-1542101), the Molecular Engineering & Sciences Institute, and the Clean Energy Institute. Part of this work was conducted at the Washington Clean Energy Testbeds, a facility operated by the University of Washington Clean Energy Institute. A portion of this work was conducted using equipment in the Biochemical Diagnostics Foundry for Translational Research supported by the M.J Murdock Charitable Trust.

REFERENCES CITED

Alvarado Flores, J. J., Alcaraz Vera, J. V., Ávalos Rodríguez, M. L., Rutiaga Quiñones, J. G., Valencia, J. E., Guevara Martínez, S. J., Ríos, E. T., and Zarraga, R. A. (2022). "Kinetic, thermodynamic, FT-IR, and primary constitution analysis of *Sargassum* spp. from Mexico: Potential for hydrogen generation," *Int. J. Hydrog. Energy* 47(70), 30107-30127. DOI: 10.1016/j.ijhydene.2022.05.051

Alves, A., Caridade, S. G., Mano, J. F., Sousa, R. A., and Reis, R. L. (2010). "Extraction and physico-chemical characterization of a versatile biodegradable polysaccharide obtained from green algae," *Carbohydr. Res.* 345(15), 2194-2200. DOI: 10.1016/j.carres.2010.07.039

Atugoda, T., Gunawardane, C., Ahmad, M., Vithanage, M. (2021). "Mechanistic interaction of ciprofloxacin on zeolite modified seaweed (*Sargassum crassifolium*) derived biochar: Kinetics, isotherm and thermodynamics," *Chemosphere* 281, article ID 130676. DOI: 10.1016/j.chemosphere.2021.130676

Bedoya-Henao, C. A., Carmona-Ramírez, J. D., Betancur-Granados, N., Cabrera-Poloche, F. D., Viana-Casas, G. A., Restrepo-Baena, O. J., and Tobón, J. I. (2025). "Characterization and potential uses of municipal solid waste incineration remnants in San Andrés Islands – Colombia," *Case Studies Chem. Env. Engr* 11, article ID 101047. DOI: 10.1016/j.cscee.2024.101047

Bhagyaraj, S., and Krupa, I. (2020). "Alginate-mediated synthesis of hetero-shaped silver nanoparticles and their hydrogen peroxide sensing ability," *Molecules* 25(3), article 435. DOI: 10.3390/molecules25030435

Bhatnagar, P., Gururani, P., Bisht, B., and Kumar, V. (2021). "Algal biochar: An advance and sustainable method for wastewater treatment," *Octa. J. Biosci.* 9(2), 2321-3663.

Bilba, K., Onésippe Potiron, C., and Arsène, M.-A. (2023). "Invasive biomass algae valorization: Assessment of the viability of Sargassum seaweed as pozzolanic

material," *J. Environ. Manage.* 342, article ID 118056. DOI: 10.1016/j.jenvman.2023.118056

Buckee, G. K. (1994). "Determination of total nitrogen in barley, malt and beer by Kjeldahl procedures and the dumas combustion method collaborative trial," *J. Inst. Brewing* 100(2), 57-64. DOI: 10.1002/jib.1994.100.2.57

Cao, B., Yuan, J., Jiang, D., Wang, S., Barati, B., Hu, Y., Yuan, C., Gong, X., and Wang, Q. (2021). "Seaweed-derived biochar with multiple active sites as a heterogeneous catalyst for converting macroalgae into acid-free biooil containing abundant ester and sugar substances," *Fuel* 285, article ID 119164. DOI: 10.1016/j.fuel.2020.119164

Coleman, A., Davis, K., DeAngelo, J., Saltiel, T., Saenz, B., Miller, L., Champion, K., Harrison, E., and Otwell, A. (2024). "2023 Billion-Ton Report. DOE BETO Report No.: Chapter 7, Emerging Resources: Microalgae, Macroalgae, and Point-Source Carbon Dioxide Waste Streams," DOI: 10.23720/BT2023/2316176

Das, O., Sarmah, A. K., and Bhattacharyya, D. (2015). "Structure–mechanics property relationship of waste derived biochars," *Sci. Total Environ.* 538, 611-620. DOI: 10.1016/j.scitotenv.2015.08.073

Das, O., Sarmah, A. K., and Bhattacharyya, D. (2016). "Nanoindentation assisted analysis of biochar added biocomposites," *Compos. Part B- Eng.* 91, 219-227. DOI: 10.1016/j.compositesb.2016.01.057

Debono, O., and Villot, A. (2015). "Nitrogen products and reaction pathway of nitrogen compounds during the pyrolysis of various organic wastes," *J. Anal. Appl. Pyrol.* 114, 222-234. DOI: 10.1016/j.jaap.2015.06.002

Dietz, T., Shwom, R. L., and Whitley, C. T. (2020). "Climate change and society," *Annu. Rev. Sociol.* 46, 135-158. DOI: 10.1146/annurev-soc-121919054614

Doh, H., and Whiteside, W. S. (2020). "Isolation of cellulose nanocrystals from brown seaweed, *Sargassum fluitans*, for development of alginate nanocomposite film," *Polym. Cryst.* 3(4), article 10133. DOI: 10.1002/pcr2.10133

Duarte, C. M., Bruhn, A., and Krause-Jensen, D. (2021). "A seaweed aquaculture imperative to meet global sustainability targets," *Nat. Sustain.* 5(3), 185-193. DOI: 10.1038/s41893-021-00773-9

El-Gendy, N. Sh., Hosny, M., Ismail, A. R., Radwan, A. A., Ali, B. A., Ali, H. R., El-Salamony, R. A., Abdelsalam, K. M., and Mubarak, M. (2024). "A study on the potential of valorizing *Sargassum latifolium* into biofuels and sustainable value-added products," *Int. J. Biomater.* 2024(1), article ID 5184399. DOI: 10.1155/2024/5184399

Fahmy, T. Y. A., Fahmy, Y., Mobarak, F., El-Sakhawy, M., and Abou-Zeid, R. E. (2018). "Biomass pyrolysis: Past, present, and future," *Environ. Dev. Sustain.* 22(1), 17-32. DOI: 10.1007/s10668-018-0200-5

Grandgeorge, P., Campbell, I. R., Nguyen, H., Brain, R., Parker, M., Edmundson, S., Rose, D., Homolke, K., Subban, C., and Roumeli, E. (2024). "Adhesion in thermomechanically processed seaweed-lignocellulosic composite materials," *MRS Bull.* 49(8), 787-801. DOI: 10.1557/s43577-024-00734-5.

Gorham, J. (2012). "NIST X-ray photoelectron spectroscopy database - SRD 20," (https://srdata.nist.gov/xps/), Accessed 29 Jan 2025. DOI: 10.18434/T4T88K

Hossain, N., Nizamuddin, S., Griffin, G., Selvakannan, P., Mubarak, N. M., and Mahlia, T. M. I. (2020). "Synthesis and characterization of rice husk biochar *via* hydrothermal carbonization for wastewater treatment and biofuel production," *Sci. Rep.* 10(1), article 18851. DOI: 10.1038/s41598-020-75936-3

Jahirul, M. I., Rasul, M., Chowdhury, A., and Ashwath, N. (2012). "Biofuels production through biomass pyrolysis —A technological review," *Energies* 5, 4952-5001. DOI: 10.3390/en5124952

Jayathilake, K. M. P. I., Manage, P. M., and Idroos, F. S. (2024). "Invasive aquatic plants as potential sustainable feedstocks for biochar production and as an innovative approach for wastewater treatment," *Nat. Environ. Pollut. Technol.* 23(2), 991-1005. DOI: 10.46488/NEPT.2024.v23i02.033

Kabakcı, S. B., and Hacıbektaşoğlu, Ş. (2017). "Catalytic pyrolysis of biomass," in: *Pyrolysis*, M. Samer (ed.), InTech Open, London, UK.

Kim, S. H., Lee, C. M., and Kafle, K. (2013). "Characterization of crystalline cellulose in biomass: Basic principles, applications, and limitations of XRD, NMR, IR, Raman, and SFG," *Korean J. Chem. Eng.* 30(12), 2127-2141. DOI: 10.1007/s11814-013-0162-0

Kozakov, A. T., Kochur, A. G., Kumar, N., Panda, K., Nikolskii, A. V., and Sidashov, A. V. (2021). "Determination of sp2 and sp3 phase fractions on the surface of diamond films from C1s, valence band X-ray photoelectron spectra and CKVV X-ray-excited Auger spectra," *Appl. Surf. Sci.* 536, article ID 147807. DOI: 10.1016/j.apsusc.2020.147807

Lee, Y., Park, J., Ryu, C., Gang, K. S., Yang, W., Park, Y.-K., Jung, J., and Hyun, S. (2013). "Comparison of biochar properties from biomass residues produced by slow pyrolysis at 500 °C," *Bioresource Technology* 148, 196-201. DOI: 10.1016/j.biortech.2013.08.135

Leng, L., Yang, L., Chen, J., Leng, S., Li, H., Li, H., Yuan, X., Zhou, W., and Huang, H. (2020). "A review on pyrolysis of protein-rich biomass: Nitrogen transformation," *Bioresource Technol.* 315, Article ID 123801. DOI: 10.1016/j.biortech.2020.123801

Li, D., Han, Z., He, Q., Yang, K., Sun, W., Liu, H., Zhao, Y., Liu, Z., Zong, C., Yang, H., *et al*. (2023). "Ultrastrong, thermally stable, and food-safe seaweed-based structural material for tableware," *Adv. Mater.* 35(1), article ID 2208098. DOI: 10.1002/adma.202208098

Li, X.-G., Lv, Y., Ma, B.-G., Wang, W.-Q., and Jian, S.-W. (2017). "Decomposition kinetic characteristics of calcium carbonate containing organic acids by TGA," *Arab. J. Chem.* 10, S2534-S2538. DOI: 10.1016/j.arabjc.2013.09.026

Lin, B. B., Ossola, A., Alberti, M., Andersson, E., Bai, X., Dobbs, C., Elmqvist, T., Evans, K. L., Frantzeskaki, N., Fuller, R. A., *et al.* (2021). "Integrating solutions to adapt cities for climate change," *Lancet Planet Health* 5(7), e479-e486. DOI: 10.1016/S2542-5196(21)00135-2

Makowska, M., and Dziosa, K. (2024). "Influence of different pyrolysis temperatures on chemical composition and graphite-like structure of biochar produced from biomass of green microalgae *Chlorella* sp.," *Environ. Technol. Innov.* 35, article ID 103667. DOI: 10.1016/j.eti.2024.103667

Malhi, Y., Franklin, J., Seddon, N., Solan, M., Turner, M. G., Field, C. B., and Knowlton, N. (2020). "Climate change and ecosystems: Threats, opportunities and solutions," *Philos. Trans. R. Soc. B- Biol. Sci.* 375(1794), article ID 20190104. DOI: 10.1098/rstb.2019.0104

Manoj, B., and Kunjomana, A. G. (2012). "Study of stacking structure of amorphous carbon by X-ray diffraction technique," *Int. J. Electrochem. Sci.* 7(4), 3127-3134. DOI: 10.1016/S1452-3981(23)13940-X

McDonald-Wharry, J., Manley-Harris, M., and Pickering, K. (2013). "Carbonisation of

biomass-derived chars and the thermal reduction of a graphene oxide sample studied using Raman spectroscopy," *Carbon* 59, 383-405. DOI: 10.1016/j.carbon.2013.03.033

Mondal, A. K., Hinkley, C., Krishnan, L., Ravi, N., Akter, F., Ralph, P., and Kuzhiumparambil, U. (2024). "Macroalgae-based biochar: preparation and characterization of physicochemical properties for potential applications," *RSC Sustain.* 2(6), 1828-1836. DOI: 10.1039/D4SU00008K

Mong, G. R., Chong, C. T., Chong, W. W. F., Ng, J.-H., Ong, H. C., Ashokkumar, V., Tran, M.-V., Karmakar, S., Goh, B. H. H., and Mohd Yasin, M. F. (2022). "Progress and challenges in sustainable pyrolysis technology: Reactors, feedstocks and products," *Fuel* 324, article ID 124777. DOI: 10.1016/j.fuel.2022.124777

Peng, W., Wu, Q., and Tu, P. (2000). "Pyrolytic characteristics of heterotrophic *Chlorella protothecoides* for renewable bio-fuel production," *Kluwer. Acad. Publ*. 13, 5-12. DOI: 10.1023/A:1008153831875

Peng, Y., Xie, E., Zheng, K., Fredimoses, M., Yang, X., Zhou, X., Wang, Y., Yang, B., Lin, X., Liu, J., *et al*. (2012). "Nutritional and chemical composition and antiviral activity of cultivated seaweed *Sargassum naozhouense* Tseng et Lu," *Mar. Drugs* 11(1), 20-32. DOI: 10.3390/md11010020

Revilla-Lovano, S., Sandoval-Gil, J. M., Zertuche-González, J. A., Belando-Torrentes, M. D., Bernardeau-Esteller, J., Rangel-Mendoza, L. K., Ferreira-Arrieta, A., Guzmán-Calderón, J. M., Camacho-Ibar, V. F., Muñiz-Salazar, R., and Ávila-López, M. C. (2021). "Physiological responses and productivity of the seaweed *Ulva ohnoi* (Chlorophyta) under changing cultivation conditions in pilot large land-based ponds," *Algal Research* 56, article 102316. DOI: 10.1016/j.algal.2021.102316

Roche, S., Yacou, C., Jean Marius, C., Ranguin, R., Francoeur, M., Taberna, P-L., Passe-Coutrin, N., and Gaspard, S. (2023). "Carbon materials prepared from invading pelagic sargassum for supercapacitors' electrodes," *Molecules* 28(15), article 5882. DOI: 10.3390/molecules28155882

Rodionova, M. V., Poudyal, R. S., Tiwari, I., Voloshin, R. A., Zharmukhamedov, S. K., Nam, H. G., Zayadan, B. K., Bruce, B. D., Hou, H. J. M., and Allakhverdiev, S. I. (2017). "Biofuel production: Challenges and opportunities," *Int. J. Hydrog. Energy* 42(12), 8450-8461. DOI: 10.1016/j.ijhydene.2016.11.125

Ross, A., Jones, J., Kubacki, M., and Bridgeman, T. (2008). "Classification of macroalgae as fuel and its thermochemical behaviour," *Bioresource Technol.* 99(14), 6494-6504. DOI: 10.1016/j.biortech.2007.11.036

Shoaib, A. G. M., Van, H.-T., Tran, D.-T., El Sikaily, A., Hassaan, M. A., and El Nemr, A. (2024). "Green algae *Ulva lactuca*-derived biochar-sulfur improves the adsorption of methylene blue from water," *Sci. Rep.* 14(1), article ID 11583. DOI: 10.1038/s41598-024-61868-9

Singh, A., Sharma, R., Pant, D., and Malaviya, P. (2021). "Engineered algal biochar for contaminant remediation and electrochemical applications," *Sci. Total Environ.* 774, article ID 145676. DOI: 10.1016/j.scitotenv.2021.145676

Singh, B., Camps-Arbestain, M., and Lehmann, J. (2017). *Biochar: A Guide to Analytical Methods*, CSIRO Publishing, Australia.

Singh, B., Singh, B. P., and Cowie, A. L. (2010). "Characterisation and evaluation of biochars for their application as a soil amendment," *Soil Res.* 48(7), article 516. DOI: 10.1071/SR10058

Song, H., Wang, J., Garg, A., Lin, X., Zheng, Q., and Sharma, S. (2019). "Potential of novel biochars produced from invasive aquatic species outside food chain in removing ammonium nitrogen: Comparison with conventional biochars and clinoptilolite," *Sustainability* 11(24), article 7136. DOI: 10.3390/su11247136

Thabet, O. A., Alenzi, F. K., Alshubramy, M. A., Alamry, K. A., Hussein, M. A., and Hoogenboom, R. (2024). "New sorbent-based hydrophobic alginic acid derivatives for fat removal in multi-pesticide residues: Analysis of a fatty food sample," *RSC Adv.* 14(4), 2491-2503. DOI: 10.1039/D3RA07442K

Tu, P., Zhang, G., Wei, G., Li, J., Li, Y., Deng, L., and Yuan, H. (2022). "Influence of pyrolysis temperature on the physicochemical properties of biochars obtained from herbaceous and woody plants," *Bioresour. Bioprocess*. 9(1), article 131. DOI: 10.1186/s40643-022-00618-z

US EPA O. (2023). "Sargassum Inundation Events (SIEs): Impacts on aquatic life and associated ecosystems," https://www.epa.gov/habs/sargassum-inundation-events-sies-impacts-aquatic-life-and-associated-ecosystems

Wallace, C. A., Afzal, M. T., and Saha, G. C. (2019). "Effect of feedstock and microwave pyrolysis temperature on physio-chemical and nano-scale mechanical properties of biochar," *Bioresource Bioprocess* 6(1), article 33. DOI: 10.1186/s40643-019-0268-2

Wang, Z., Li, J., Yu, F., Yan, B., and Chen, G. (2021). "Comprehensive evaluation of gradient controlled anaerobic digestion and pyrolysis integration processes: A case study of *Sargassum* treatment," *Bioresource Technol.* 345, article ID 126496. DOI: 10.1016/j.biortech.2021.126496

Wu, Y., Cheng, H., Pan, D., Zhang, L., Li, W., Song, Y., Bian, Y., Jiang, X., and Han, J. (2021). "Potassium hydroxide-modified algae-based biochar for the removal of sulfamethoxazole: Sorption performance and mechanisms," *J. Environ. Manage.* 293, article ID 112912. DOI: 10.1016/j.jenvman.2021.112912

Zadeh, Z. E., Abdulkhani, A., Aboelazayem, O., and Saha, B. (2020). "Recent insights into lignocellulosic biomass pyrolysis: A critical review on pretreatment, characterization, and products upgrading," *Processes* 8(7), article 799. DOI: 10.3390/pr8070799

Zhao, M., Ma, X., Liao, X., Cheng, S., Liu, Q., Wang, H., Zheng, H., Li, X., Luo, X., Zhao, J., *et al*. (2022). "Characteristics of algae-derived biochars and their sorption and remediation performance for sulfamethoxazole in marine environment," *Chem. Eng. J.* 430, article ID 133092. DOI: 10.1016/j.cej.2021.133092

Article submitted: February 7, 2025; Peer review completed: March 9, 2025; Revised version received: April 5, 2025; Accepted: April 6, 2025; Published: April 15, 2025.
DOI: 10.15376/biores.20.2.4152-4173